清水建設研究報告
第76号平成14年10月

自己収縮と水和熱膨張による高強度コンクリートの連成ひずみと柱部材の応力

橋田　浩　(技術研究所)
山崎　庸行　(技術研究所)

Strain Composed of Autogenous Shrinkage and Thermal Expansion Due to Hydration of High Strength Concrete and Stress in Reinforced Columns

by **Hiroshi Hashida** and **Nobuyuki Yamazaki**

Abstract

Reinforced concrete members made of high strength concrete (HSC) are subjected to stress due to coupled strain resulting from autogenous shrinkage and thermal expansion/contraction, which may cause severe cracking at early age. In the paper, the coupled strain of HSC was measured and estimated, then actual strain and shrinkage stress in full-scale model columns were investigated. By taking account of the increase of thermal expansion coefficient with age, it was possible to estimate the coupled strain of HSC. While autogenous shrinkage of concrete with usual Portland cement subjected to a high temperature history was considered to be smaller than that of 20°C-curing, autogenous shrinkage of concrete with admixtures was considered to be larger when the admixture content was high. The actual strain and stress in the reinforced concrete members could be estimated based on the concept of coupled strain of HSC.

概　要

高強度コンクリートを用いた鉄筋コンクリート部材は、自己収縮と水和熱膨張／収縮による連成ひずみに起因する拘束応力が発生し、早期にひび割れる危険がある。本報告では、各種高強度コンクリートを対象に、これらの連成ひずみを把握、定量化すると共に、実規模モデル柱部材の実ひずみならびに鉄筋拘束応力について検討した。その結果、材齢に伴う線膨張係数の増大を仮定することで、高強度コンクリート部材の自己収縮ならびに水和熱膨張との連成ひずみを合理的に予測することができた。水和熱による高温履歴を受けると、ポルトランドセメント系コンクリートでは、20℃養生に比べ、自己収縮ひずみ増進は停滞する一方、混和量が多い混合セメント系コンクリートでは自己収縮ひずみは増大する。このような高強度コンクリートの連成ひずみを考慮することで、鉄筋コンクリート部材の実ひずみならびに拘束応力を算定することが可能となる。

§ 1. Introduction

The number of reinforced concrete structures made of high strength concrete (HSC) with a design strength of more than 60 N/mm^2 has been increasing in Japan. Though members made of such concrete basically exhibit high strength and high durability, they are vulnerable to early cracking. The high cement content causes a large temperature rise during early hydration, while autogenous shrinkage is at the same time also a matter of concern. For this reason, the reinforced concrete members are subjected to stress due to deformation composed of autogenous shrinkage and thermal expansion/contraction, leading to cracking. However, few studies have dealt with the coupled deformation and stress of HSC members at early ages [1)-4)].

Accordingly, the authors measured the coupled strain of HSC specimens under semi-adiabatic curing and estimated both components, autogenous shrinkage and thermal expansion. Actual strain and the shrinkage stress in full-scale model columns were then investigated by comparing the estimated values with the experimental measurements.

§ 2. Experimental Procedure

2.1 Laboratory Test

The materials of HSC are given in Table 1 and proportioned as shown in Table 2. Four types of cement or

Table 1 Materials of Concrete

Materials	Desig-nations	Kind / Characteristics
Cement	OPC	Ordinary Portland cement Density=3.16 g/cm^3, Blaine=0.327 m^2/g
	BPC	Belite-rich Portland cement (C_2S=46%) Density=3.20 g/cm^3, Blaine=0.411 m^2/g
	OBC	Blastfurnace slag cement B type Density=3.04 g/cm^3, Blaine=0.370 m^2/g (OPC replaced about 42 wt% by slag)
Silica fume	SF	Density=2.20 g/cm^3, Blaine=20 m^2/g
Fine aggregate	S	Land sand / Density=2.59, Absorption=1.63%, F. M.=2.80
Coarse aggregate	G	Crushed sand stone / Max. size=20mm Density=2.65, Absorption=0.60%
Chemical admixture	SP	Air entraining and high-rage water reducing agents

Table 2 Mix Proportions

Mix	W/B (%)	W	C	SF	S	G	f_{cs} (N/mm^2)
		kg/m^3					
BPC40	40	168	420	—	785	975	76.8
BPC27	27	165	611	—	697	940	101
BPC20	20	165	825	—	581	896	119
BSC20	20	165	784	41	606	856	123
OPC40	40	168	420	—	780	975	68.2
OPC27	27	165	611	—	692	940	97.4
OPC20	20	165	825	—	573	896	109
OBC27	27	165	611	—	751	859	109

binder were used: ordinary Portland cement (OPC), belite-rich Portland cement (BPC), BPC with 5% replaced by mass with silica fume (BSC) and blast furnace slag cement (OPC with about 42% replaced by mass with slag, OBC). Eight types of concrete were prepared, with OPC or BPC having a water-cement ratio (W/C) of 0.40, 0.27, and 0.20, BSC having a water-binder ratio (W/B) of 0.20 and OBC having a W/C of 0.27. The belite (C_2S) content of BPC was 46% in terms of mineral composition. Table 2 also shows the averages of the 28-day compressive strength, f_{cs} of standard-cured specimens.

The changes in the autogenous shrinkage strain and pore humidity at a constant temperature of 20°C and the total strain under semi-adiabatic curing, i.e. the strain composed of autogenous shrinkage and thermal expansion, were measured. The autogenous shrinkage and pore humidity test at 20°C were conducted using beam specimens 100×100×400 mm and cylinders ϕ100×200 mm in size as shown in Figure 1 and 2. For the semi-adiabatic curing test, beam specimens 100×100×700 mm in size were fabricated using molds made of insulation as shown in Figure 3. They were adiabatic-cured from immediately after placing to undergo a temperature history similar to the actual members. The strains and temperatures of beam specimens were measured with

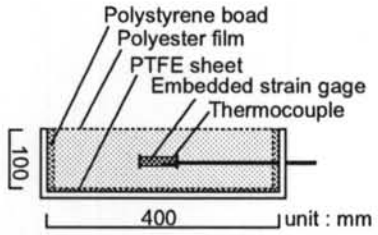

Fig. 1 Test Specimen for Measurement of Autogenous Shrinkage Cured at 20°C

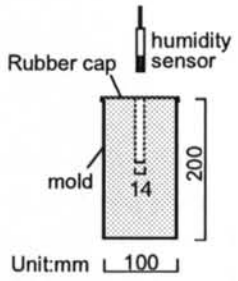

Fig. 2 Test Specimen for Measurement of Pore Humidity Cured at 20°C

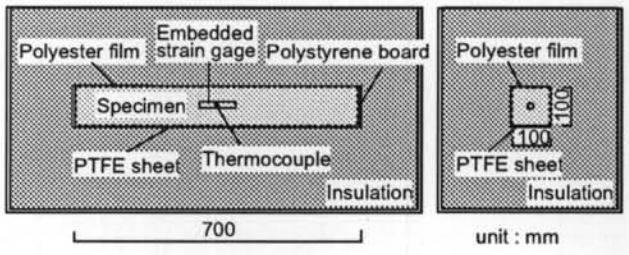

Fig. 3 Test Specimen for Semi-adiabatic Curing

embedded strain gauges and thermocouples.

2.2 Experiments on Full-scale Columns

Two types of ready-mixed concrete, OPC-Rm and BPC-Rm with materials and mix proportions (Table 3) similar to OPC27 and BPC27 in the laboratory test, were used for an experiment on full-scale columns. For the experiment, unreinforced and reinforced concrete model columns (U-column and R-column) 550×600 mm in cross section and 1500 mm in height were prepared as shown in Figure 4. Whereas the U-column was used for measuring the total strain composed of autogenous shrinkage, thermal expansion and

Table 3 Mix Proportions of RMC

Mix	W/C (%)	W	C	S	G	f_{cs} (N/mm^2)
		kg/m^3				
BPC-Rm	27	170	630	741	854	92.7
OPC-Rm	28	165	589	719	922	96.1

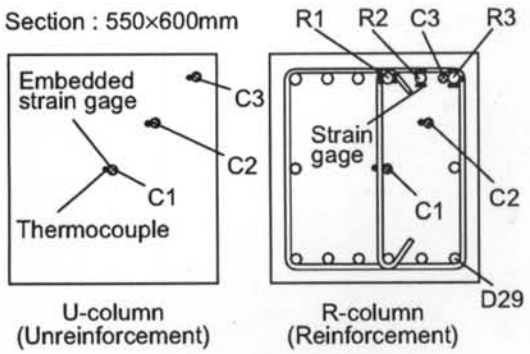

Fig. 4 Full-scale Model Columns

internally restricted strain, the R-column was used for measuring the actual strain of the main reinforcing bar and concrete under restraint of the reinforcing bar. To minimize the effect of drying, the exposed surfaces of the wooden formwork were covered with curing sheets. The placing surface of OPC-Rm, however, was exposed to the air by mistake, while that of BPC-Rm was covered with curing sheets from immediately after placing. The strains of concrete and the reinforcing bar were measured with embedded strain gauges and foil strain gauges (the 4 gauge method), respectively. The measuring points for strain and temperature are shown in the cross sectional view in Figure 4. Measurements were made at 3 heights, but this paper deals with only the central measuring point readings.

§ 3. Results

3.1 Autogenous Shrinkage at 20°C

The autogenous shrinkage strains of specimens cured at 20°C are shown in Figure 5. In this paper, the datum strain of the autogenous shrinkage is the value at the time of final setting because final setting nearly corresponds to the practical revelation of elasticity and stress of concrete. The autogenous shrinkage developed to 50% of the 28-day value by an equivalent age of 1 day and gradually converged. When comparing specimens with the same water-cement ratio, the autogenous shrinkage strain of BPC specimens was much lower than OPC specimens, presumably due to the C_3A content of belite-rich cement as low as approximately 3% [2]. The autogenous shrinkage strain can be approximated by the model curve of equation (1).

$$\varepsilon_{as}(t) = \varepsilon_{ass} \cdot \exp\left\{ s_\varepsilon \left[1 - \left(\frac{28 - t_{fs}}{t - t_{fs}} \right)^{0.5} \right] \right\} \qquad (1)$$

where $\varepsilon_{as}(t)$= autogenous shrinkage strain at t days, t = equivalent age (days), ε_{ass}= autogenous shrinkage strain at 28 days, s_ε= factor for rate of autogenous shrinkage development and t_{fs}= final setting time (days). The equivalent age used in the paper is specified in CEB-FIP Model Code 90 [5] and expressed by equation (2).

$$t_T = \sum_{i=1}^{n} \Delta t_i \cdot \exp\left[13.65 - \frac{4000}{273 + T(\Delta t_i)} \right] \qquad (2)$$

where t_T= equivalent age (days), $T(\Delta t_i)$= temperature in period Δt_i(°C) and Δt_i= duration of temperature T (days). The solid lines in Figure 5 are the autogenous shrinkage strain curves at 20°C approximated by Equation (1). The values of ε_{ass} and s_ε regressed for each concrete are listed in Table 4. These parameters are significantly dependent on the water-cement ratio.

Figure 6 shows the changes in the pore humidity of concrete in an environment at 20°C. The humidity of all concretes progressively decreased over time. Those of BPC20, BSC20, OPC20, and OBC27 particularly decreased to around 75%RH at 3 months, clearly exhibiting self-desiccation due to hydration. Figure 7 shows the relationship between the pore humidity and autogenous shrinkage, exhibiting

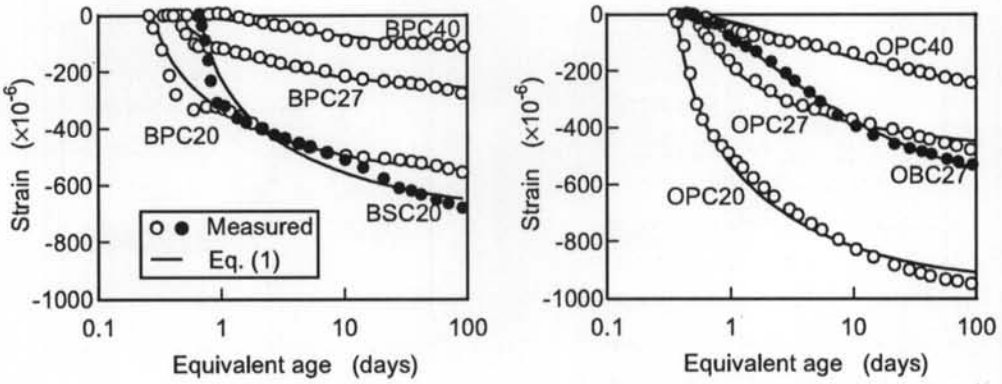

Fig. 5 Autogenous Shrinkage Strains of Specimens at 20°C

Table 4 ε_{ass} and s_ε Regressed by Euation (1)

Mix	BPC40	BPC27	BPC20	BSC20	OPC40	OPC27	OPC20	OBC27
$\varepsilon_{ass}(\times 10^{-6})$	98	236	512	610	193	420	900	473
s_ε	0.37	0.13	0.09	0.13	0.37	0.13	0.09	0.32

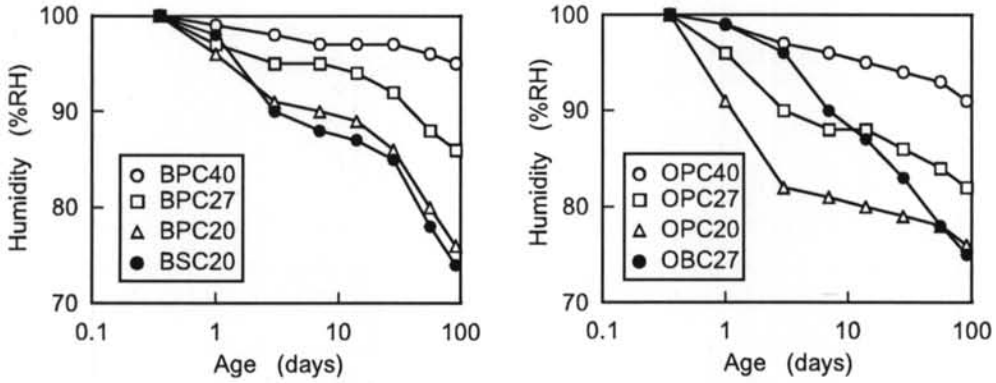

Fig. 6 Pore Humidity Changes of Specimens at 20°C

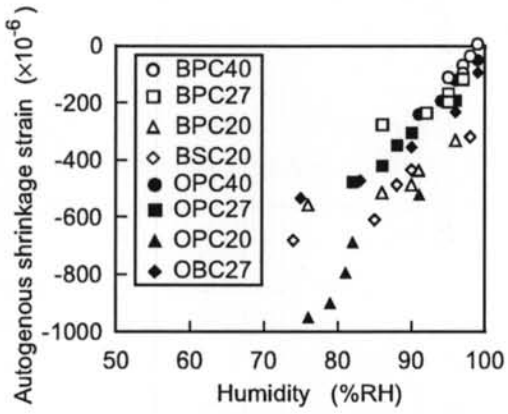

Fig. 7 Pore Humidity versus Autogrnous Shrinkage

correlation, though some types show certain scatter. It is therefore considered that autogenous shrinkage of HSC significantly depends on the self-desiccation.

3.2 Coupled Strain under Semi-adiabatic Curing

Figure 8 shows the temperature histories and of the specimensthe under semi-adiabatic curing and Figure 9 shows the changes in the total strain of the specimens, i.e. the coupled strain from autogenous shrinkage and thermal expansion/contraction. These temperature histories are very similar to those of the full-scale model columns (see Figure 10).

The datum strain for plotting the coupled strain was also the value at the time of final setting. The solid lines in Figure 9 show the changes in the strain due to autogenous shrinkage at 20°C (e_{as20}) superposed on the thermal expansion (e_{therm}). Thermal expansion coefficients were measured by subjecting post-test specimens to temperature changes at an age of 3 months, when the autogenous shrinkage had almost converged. They widely varied from one concrete to another,

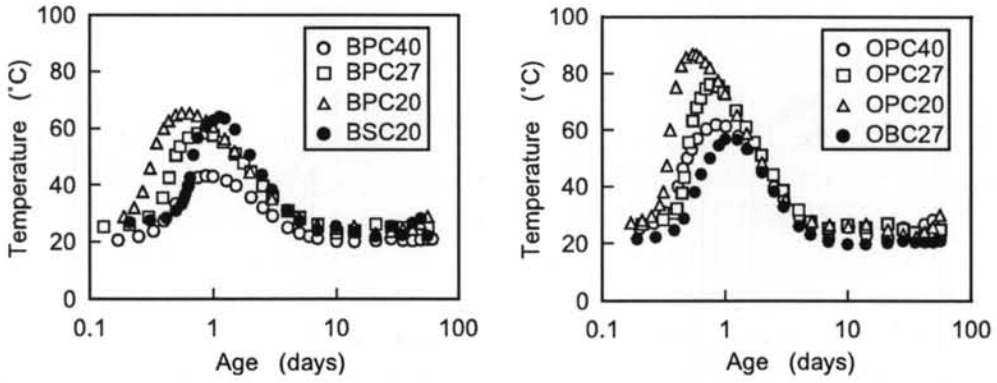

Fig. 8 TemperatureHistories under Semi-adiabatic Curing

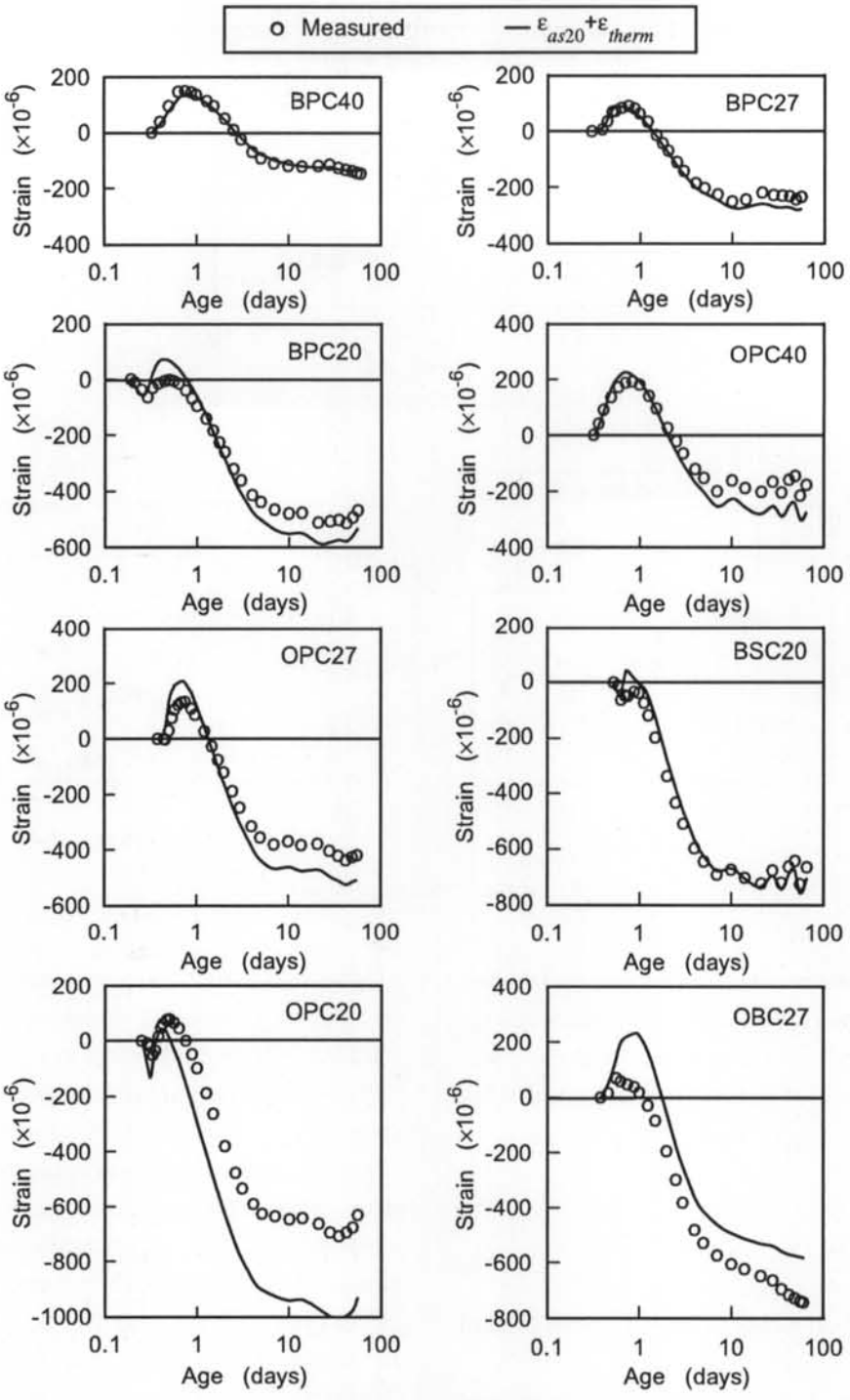

Fig. 9 Coupled Strains under Semi-adiabatic Curing

ranging from 8.0 to 13.3×10⁻⁶/°C (see Figure 14). In the case of BPC40, BPC27 and BSC20, there were small differences between the superposed strain and the measurement. In the case of BPC20, OPC40 and OPC27, the differences were moderate, whereas in the case of OPC20 and OBC27, the differences were great. These may result from the differences in autogenous shrinkage development and thermal expansion coefficients through semi-adiabatic curing.

3.3 Actual Strain in Full-scale Model Columns

Temperature histories of the full-scale model members, U-columns which had much the same histories as R-columns, are shown in Figure 10. Figure 11 shows the actual strain changes of concrete measured in U-columns and those of reinforcing bars measured in R-columns. Accordance of the strain changes from the center (C1) to the corner (C3) demonstrates that the plane section of the column remains plane under the temperature histories. The difference in actual

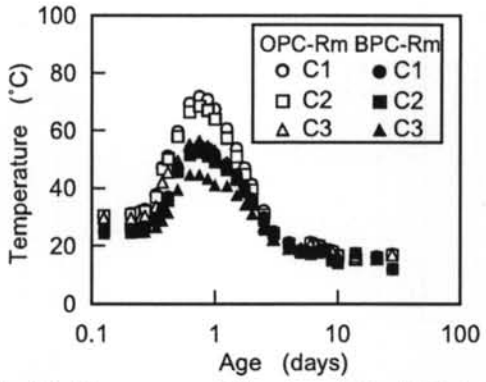

Fig. 10 Temperature Histories of Model Columns

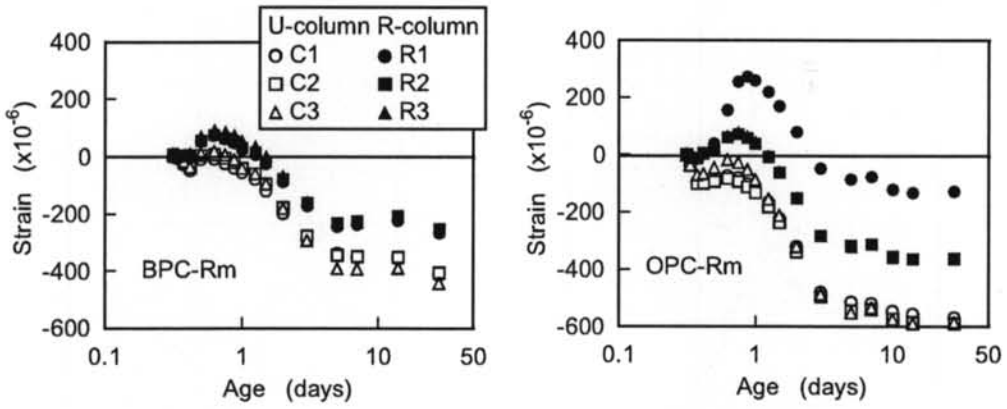

Fig. 11 Actual Strains of Model Columns

strain between the concrete in U-columns and the reinforcing bars in R-columns was considered to cause the shrinkage stress of concrete in R-columns. Some shrinkage cracks tended to relax the strain of R1 bar in R-columns with OPC-Rm.

§ 4. Discussion

4.1 Coupled Strain from Autogenous shrinkage and Thermal expansion

As shown in Figure 9, the actual changes in the strain of HSC subjected to high temperatures differ from the superposed strain consisting of the autogenous shrinkage at 20°C and the thermal expansion. One reason for the difference may be that the actual thermal expansion coefficient is not constant throughout the ages. However, the thermal expansion coefficient of HSC at early ages has scarcely been measured, as the simultaneous autogenous shrinkage strain makes it difficult to identify. Nevertheless, it is reported that the thermal expansion coefficient of cement paste increases with age [6] and is highest when the relative humidity is around 70% [7]. It is therefore expected that the thermal expansion coefficient of HSC with a large autogenous shrinkage, i.e. large self-desiccation, increases with age as shown in Figure 12, referring to the results measured by Bjøntegaard & Sellevold [3]. It was considered that the thermal expansion coefficient of concrete is great before the final setting, as the thermal expansion coefficient of water is large and the fabric of the microstructures has not been fully formulated. The thermal expansion coefficient is considered minimized near the final setting, when the fabric has been formed and the concrete is still in a wet condition. Also, it is judged rational to assume the thermal expansion coefficient at the final setting to be 7.0×10^{-6}/°C, since the pore humidity correlates with the thermal expansion coefficient regardless of concrete types as evidently shown in Figure 13. Accordingly, as a case study hereafter, the coefficient of thermal expansion, a, was assumed to be 7.0×10^{-6}/°C at the final setting and increases in proportion to the logarithm of the age up to an age of 3 months as shown in Figure 14 and expressed by equation (3).

$$\alpha(t) = a_1 \ln(t / t_{fs}) + b_1 \qquad (3)$$

where $\alpha(t)$ = coefficient of thermal expansion at t days (1/°C), t = equivalent age (days), t_{fs} = final setting time (days),

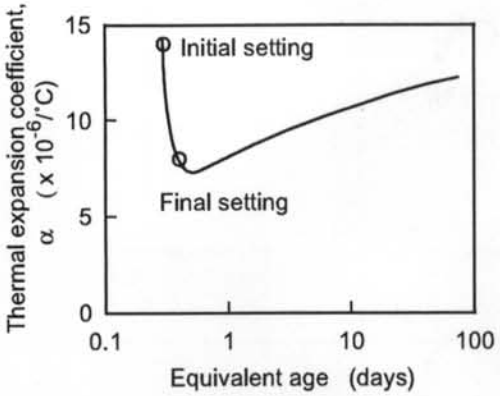

Fig.12 Concept of Coefficient of Thermal Expansion at Early Age

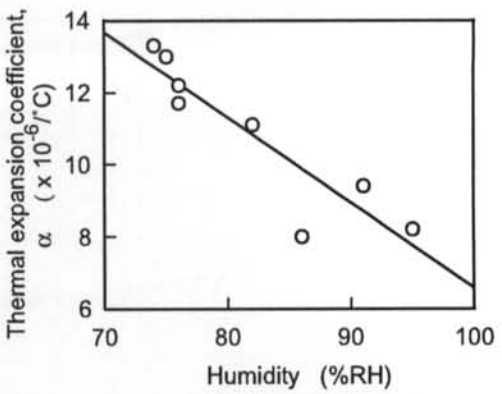

Fig. 13 PoreHumidity versus Coefficient of Thermal Expansion

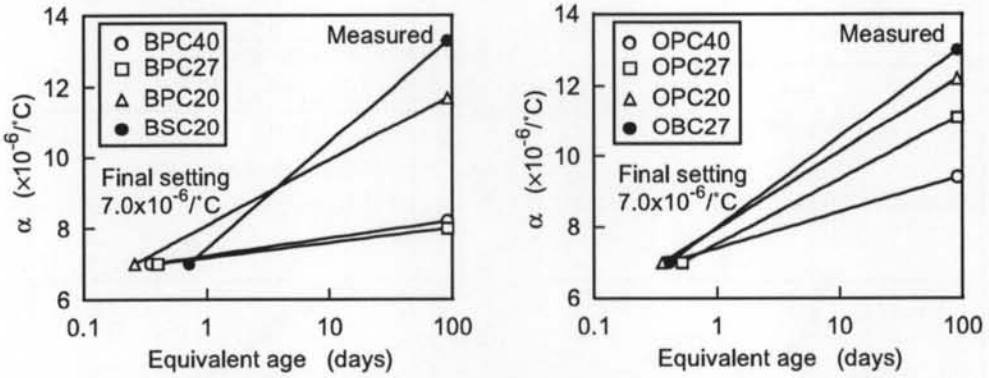

Fig. 14 Assumed Coefficients of Thermal Expansion, α, as a Case Study

coefficients a_1 and b_1 = material constans and $b_1 = 7.0\times10^{-6}$ in this study.

Figure 15 shows separations of the actual strains of OPC27 under semi-adiabatic curing into thermal strains and autogenous shrinkage strains, with the coefficient of thermal expansion being assumed in one case to be constant at the measurement at an age of 3 months and in another case to be increasing according to Figure 14. A nearly exponential curve of autogenous shrinkage strain was obtained when the increasing coefficient of thermal expansion was applied, whereas a wavy and unreasonable strain curve was obtained when the constant coefficient was applied. The development of the exponential strain curve became about 64% of that of 20°C-curing. Figure 16 shows the autogenous shrinkage strains of other concretes with OPC or BPC, also suiting to exponential curves when the increasing coefficient was

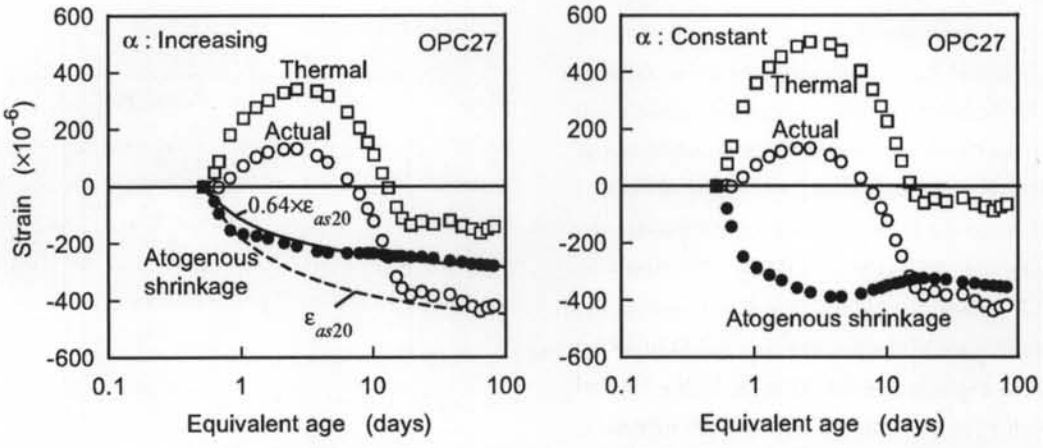

Fig. 15 Separations of Actual Strain of OPC27 under Semi-adiabatic Curing into Thermal Strain and Autogenous Shrinkage Strain

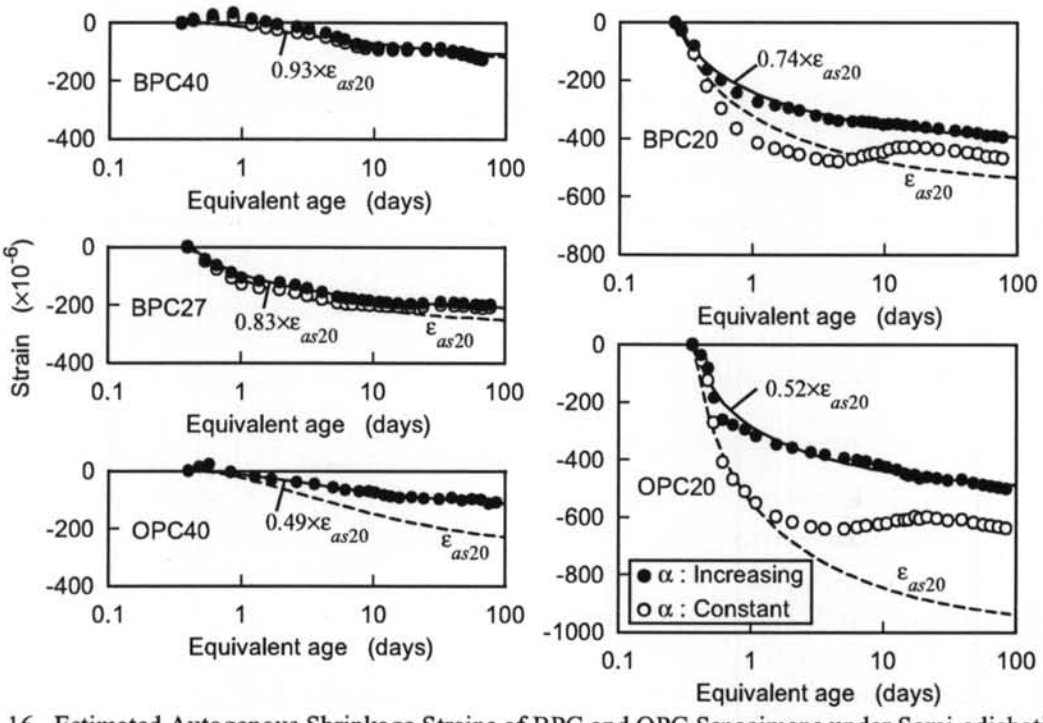

Fig. 16 Estimated Autogenous Shrinkage Strains of BPC and OPC Sspecimens under Semi-adiabatic Curing

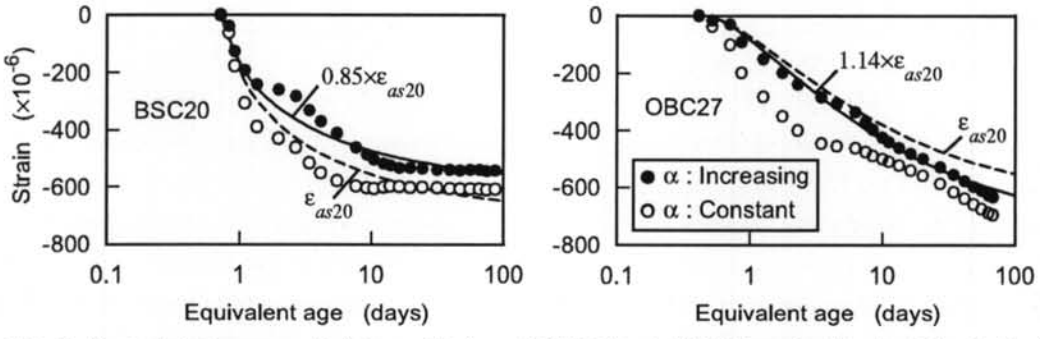

Fig. 17 Estimated Autogenous Shrinkage Strains of BSC20 and OBC27 under Semi-adiabatic Curing

applied. The exponential strain curves were about 49-93% of that of 20°C-curing in all cases. In other words, autogenous shrinkage strain remains lower when subjected to a high temperature history at early ages than when maintained at 20°C, similarly to strength development. These results in the case study suggest that by taking account of the increase in the coefficient of thermal expansion, reasonable autogenous shrinkage curves suiting to exponential functions are obtained. Figure 17 shows the autogenous shrinkage strains of OBC27 and BSC20, also suiting to exponential curves but having some complexity even when the increasing coefficient was applied. Figure 18 shows the relationship between the maximum temperature in the history and the ratio of the development of autogenous shrinkage in the history to that of 20°C-curing (e_{as}/e_{as20}). Though the amount of data is limited, the figure clearly reveals that the autogenous shrinkage of HSC with usual Portland cements is highly dependent on the temperature conditions regardless of the cement type. Therefore $\varepsilon_{as}/\varepsilon_{as20}$ of such concrete may be roughly expressed by equation (4).

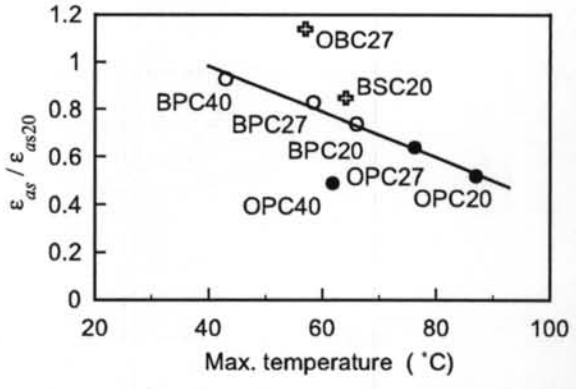

Fig. 18 Effect of Maximum Temperature on Autogenous Shrinkage

$$\varepsilon_{as}/\varepsilon_{as20} = -0.0095 \cdot T_{\max} + 1.36 \quad (T_{\max} \geq 40^{\circ}C) \qquad (4)$$

where $T_{\max}$= maximum temperature of concrete during curing (°C).

It should be noted, however, that OBC27 and BSC20 show higher developments, especially OBC27 is higher than 1.0, presumably due to the fact that temperature has a great influence on the hydrating activity and hydrated microstructure of admixtures such as blast furnace slag and silica fume. The singularly low development of OPC40 cannot easily be evaluated and requires further investigation.

4.2 Estimation of Actual Strain and Stress in Columns

Figure 19 shows the autogenous shrinkage strains of OPC-Rm and BPC-Rm at 20°C measured in the same manner as the laboratory test. The lines in the figure are the strain curves approximated by equation (1). The strain curves at 20°C and the temperature changes measured were the basic data to estimate the actual strain and stress in the model columns. For the actual strain in the U-column, we roughly estimated the temperature change at the boundary (CB in Figure 20) where the internally restricted thermal stress is assumed to hardly occur. Then the coupled strain from autogenous shrinkage and thermal expansion at the boundary, which meant the actual strain in the U-column, was estimated through the process as described above. For the actual strain and the average stress of concrete in the R-column, we applied the step-by-step method based on the principle of superimposition of creep and on the self-equilibrium between concrete and reinforcing bars. The stresses of concrete at the center (C1) and at the corner (C3) were estimated based on the difference between the actual strain and the coupled strain at each point. The principle of the estimating process is shown in Figure 20.

Elastic modulus and creep coefficient required for the estimation were determined with the following equations, referring to previous papers [1), 8)]:

$$E_c(t) = E_{cs} \cdot \exp\left\{ s_E \left[1 - \left(\frac{28 - t_{fs}}{t - t_{fs}} \right)^{0.5} \right] \right\} \qquad (5)$$

where $E_c(t)$= elastic modulus at t days, t = equivalent age (days), E_{cs}= 28-day elastic modulus of standard-cured specimen, s_E= factor for rate of elastic modulus development and t_{fs}= final setting time (days).

$$\phi(t,t_0) = \phi_0 \frac{(t-t_0)^{0.6}}{\beta + (t-t_0)^{0.6}} \qquad (6)$$

where $\phi(t,t_0)$= creep coefficient at t days of specimen loaded at t_0 days, t and t_0= equivalent age (days), ϕ_0= apparent ultimate creep coefficient determined by equation (7) and β= factor for rate of creep progress determined by equation (8).

$$\phi_0 = b_2 - a_2 \frac{E_c(t_0)}{E_{cs}} \qquad (7)$$

$$\beta = 0.05 \exp\left[5.0 \frac{E_c(t_0)}{E_{cs}} \right] \qquad (8)$$

where coefficients a_2 and b_2 = material constans. As seen from the equations above, the creep coefficient was determined as a function of elastic modulus. The coefficients, factors and measurements of BPC-Rm and OPC-Rm inputted in the equations are listed in Table 5. The estimation of the actual strain and the stress of concrete in the R-column was done with the following equations:

step-by-step method;

$$\sigma_c(t_{i+1/2}) = \frac{1}{J(t_{i+1/2}, t_i)} \left[\varepsilon_c(t_{i+1/2}) - \varepsilon_{c\epsilon}(t_{i-1/2}) - \varepsilon_{co}(t_{i+1/2}) \right] \qquad (9)$$

where,

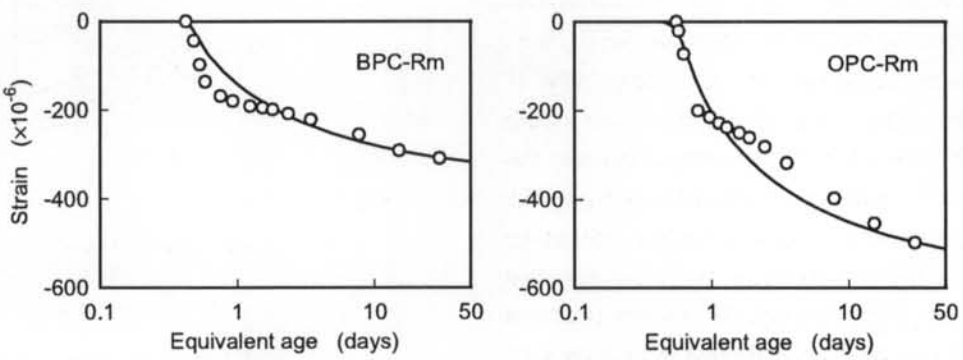

Fig. 19 Autogenous Shrinkage Strains of OPC-Rm and BPC-Rm at 20°C

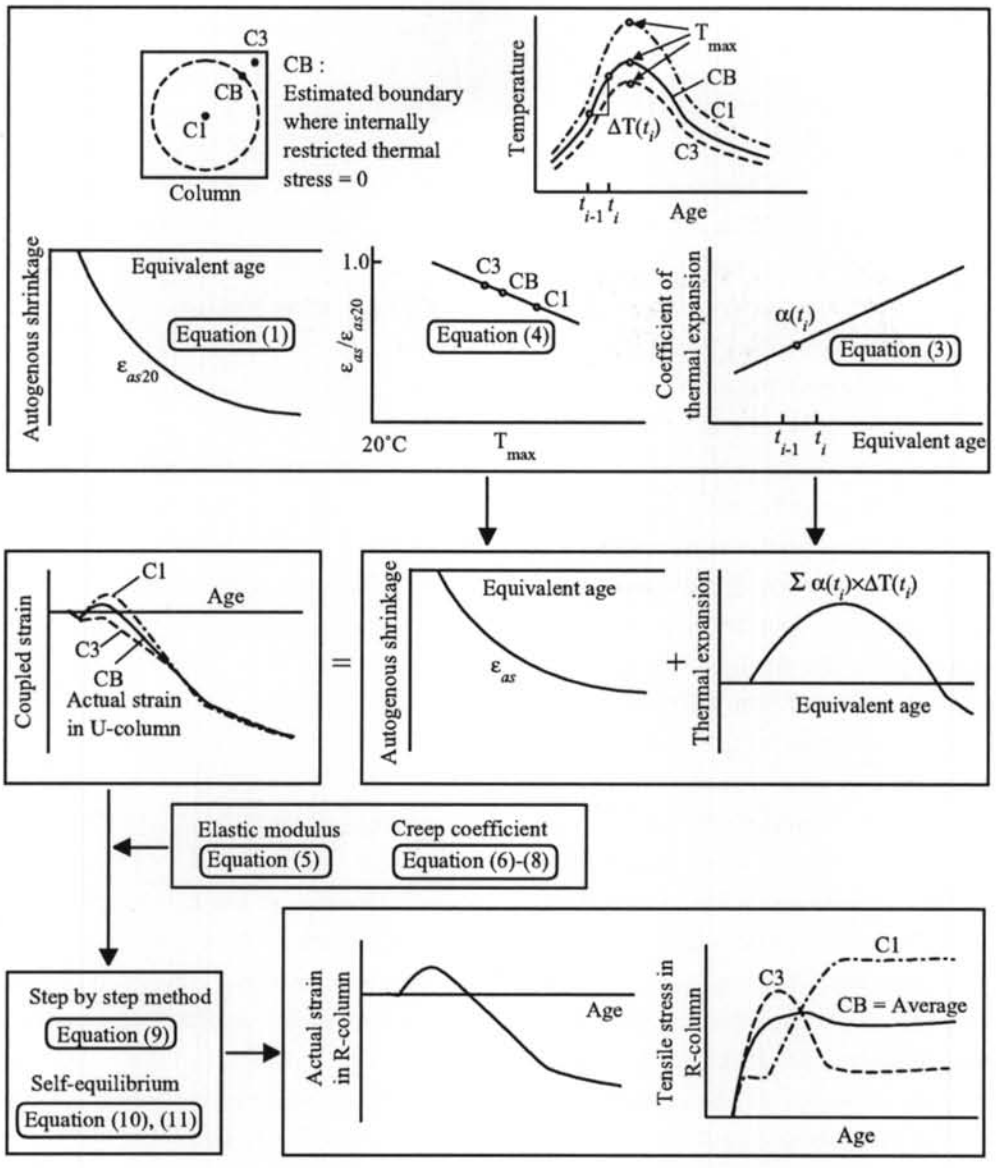

Fig. 20 Flow Chart, in Principle, for Estimation

Table 5 Coefficients and Measurements of BPC-Rm, OPC-Rm Used for Estimation

Coefficient/ Mesurement	Eq. (1)			Eq. (3)		Eq. (4) : at CB		Eq. (5)		Eq. (7)	
	ε_{ass} ($\times 10^{-6}$)	s_ε	$t_{\beta t}$ (day)	a_1 ($\times 10^{-6}$)	b_1 ($\times 10^{-6}$)	T_{max} (°C)	$\varepsilon_{as}/\varepsilon_{as20}$	E_{cs} (kN/mm^2)	s_E	a_2	b_2
BPC-Rm	307	0.13	0.40	0.37	7.0	50	0.89	36.8	0.115	4.0	4.9
OPC-Rm	495	0.13	0.51	0.77	7.0	64	0.75	39.2	0.075	4.9	5.8

$$J(t_{i+1/2},t_i)=\frac{1}{E_c(t_i)}+\frac{\phi(t_{i+1/2},t_i)}{E_{cs}},$$

$$\varepsilon_{ce}(t_{i-1/2})=\sum_{j=1}^{i-1}\Delta\sigma_c(t_j)\cdot J(t_{i+1/2},t_j)-\sigma_c(t_{i-1/2})\cdot J(t_{i+1/2},t_i),$$

$$\Delta\sigma_c(t_i)=\sigma_c(t_{i+1/2})-\sigma_c(t_{i-1/2}),$$

$t_{i-1/2}$, t_i and $t_{i+1/2}$= at the beginning, the middle and the end of i th time interval, $\sigma_c(t_{i+1/2})$= stress of concrete at time $t_{i+1/2}$, $\varepsilon_c(t_{i+1/2})$= actual strain of concrete at time $t_{i+1/2}$ and $\varepsilon_{co}(t_{i+1/2})$= coupled strain at time $t_{i+1/2}$.

self-equilibrium condition;

$$A_c\cdot\sigma_c(t_{i+1/2})+A_s\cdot E_s\left[\varepsilon_s(t_{i+1/2})-\varepsilon_{sT}(t_{i+1/2})\right]=0 \quad (10)$$

$$\varepsilon_c(t_{i+1/2})=\varepsilon_s(t_{i+1/2}) \quad (11)$$

where A_c= sectional area of concrete, A_s= total sectional area

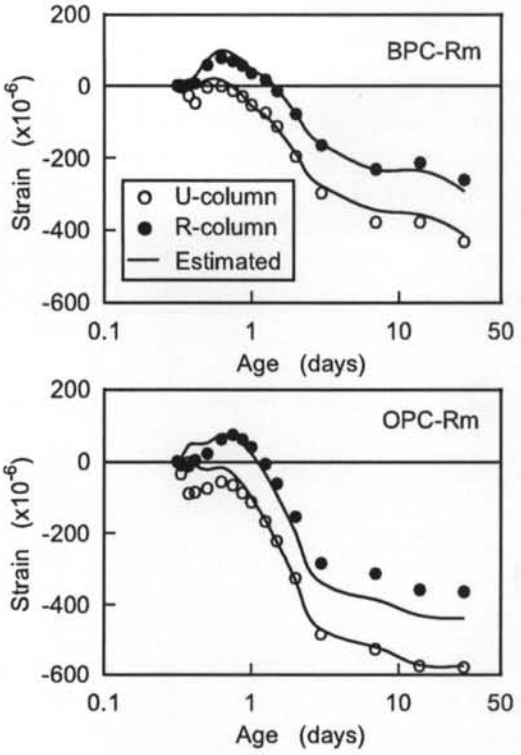

Fig. 21 Measured and Estimated Actual Strains in Columns

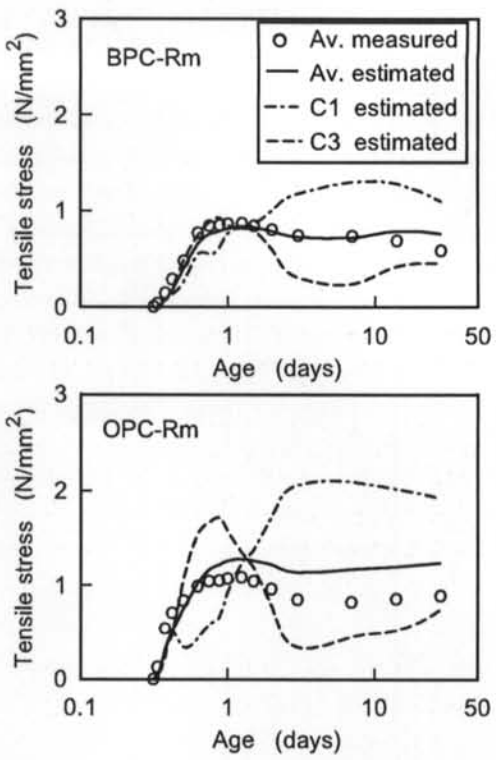

Fig. 22 Measured and Estimated Stresses in R-columns

of main bars, E_s= elastic modulus of main bar, $\varepsilon_s(t_{i+1/2})$= actual strain of main bar at time $t_{i+1/2}$ and $\varepsilon_{sT}(t_{i+1/2})$= thermal strain of main bar at time $t_{i+1/2}$.

Figure 21shows the measured and the estimated actual strains in U-columns and R-columns. Each measured value was the average of three measurements, C1-C3 or R1-R3. The measured and the estimated values agree enough except OPC-Rm after the age of 2 days in R-column, probably due to cracking. Figure 22 shows the measured average stress, converted from the strain of reinforcing bar, and the estimated stress in R-columns. While the average stress estimated of BPC-Rm agrees well with the measured one, that of OPC-Rm overestimates the measured one, corresponding with cracking. It was considered that the stress at the corner (C3) of OPC-Rm up to the age of 1 day was too high to protect against the crack.

These results make clear that the estimating approach including the concept of strain composed of autogenous shrinkage and thermal expansion are very useful for the analysis of actual strain and stress of HSC structural members.

§ 5. Conclusions

Autogenous shrinkage strain and coupled strain resulting from autogenous shrinkage and thermal expansion of HSC specimens were experimentally investigated. Then the actual strain and stress in full-scale model columns of HSC were experimentally and analytically investigated. Though the amount of data is limited, the following were found:

1) Autogenous shrinkage strain beginning at final setting was obtained, and its practical development model was proposed.

2) By taking account of the increase of thermal expansion coefficient with age, it was possible to estimate coupled deformation due to autogenous shrinkage and thermal expansion of HSC subjected to a high temperature history at early ages, such as structural members.

3) While autogenous shrinkage of concrete with usual Portland cement subjected to a high temperature history was considered to be smaller than that of 20°C-curing, autogenous shrinkage of concrete with mineral admixtures, such as silica fume and blast furnace slag, was considered to be larger when the admixture content was high.

4) The actual strain and stress in the reinforced concrete columns could be estimated based on the concept of coupled deformation.

References

1) Tomosawa, F., Noguchi, T., Park, Q.B., Sano, H., Yamazaki, N., Hashida, H. & Kuroda, Y., Experimental determination and analysis of stress and strain distribution of reinforced high-strength concrete column caused by self-desiccation and heat of hydration, Self-desiccation and its importance in concrete technology, Rep. TVBM-3075, Lund Inst. of Technology, Lund, (1997) 174-192.
2) Technical committee on autogenous shrinkage of concrete (TCASC), Japan Concrete Institute, Committee rep. Proc, Intern. Workshop on Autogenous Shrinkage of Concrete, Hiroshima, 1998 (Ed. by Tazawa, E., 1999) 1-62.
3) Bjøntegaard, Ø. & Sellevold, E.J., Thermal Dilation-Autogenous shrinkage: How to separate? Proc, Intern. Workshop on Autogenous Shrinkage of Concrete, Hiroshima, 1998 (Ed. by Tazawa, E., 1999) 245-256.
4) Hedlund, H. & Westman, G.: Autogenous deformations and stress development in hardening concrete, Proc, Intern. Workshop on Autogenous Shrinkage of Concrete, Hiroshima, 1998 (Ed. by Tazawa, E., 1999) 339-350.
5) CEB-FIP Model Code 1990.
6) Wittmann, F. & Lukas, J., Experimental study of thermal expansion of hardened cement paste. Materials and Structure 7(40), (1974) 247-252.
7) Neville, A.M., Properties of Concrete, 3rd Edition. Longman Scientific & Technical, (1986) 493 pp.
8) Hashida, H. & Yamazaki, N., A calculation method of autogenous shrinkage stress in high-strength concrete structures subjected to elevated temperature at early age, J. Struct. Constr. Eng., AIJ, No.537, (2000) 7-12 (In Japanese).